Steel and Composite Structures, *Vol. 35, No. 3* (*2020*) *449-462*
DOI: https://doi.org/10.12989/scs.2020.35.3.449

Free axial vibration of cracked axially functionally graded nanoscale rods incorporating surface effect

Reza Nazemnezhad*[1] and Hassan Shokrollahi[2a]

[1]*School of Engineering, Damghan University, Damghan, Iran*
[2]*Department of Mechanical Engineering, Faculty of Engineering, Kharazmi University, Tehran, Iran*

(*Received September 18, 2019, Revised March 17, 2020, Accepted April 3, 2020*)

Abstract. This work aims to study effects of the crack and the surface energy on the free longitudinal vibration of axially functionally graded nanorods. The surface energy parameters considered are the surface stress, the surface density, and the surface Lamé constants. The cracked nanorod is modelled by dividing it into two parts connected by a linear spring in which its stiffness is related to the crack severity. The surface and bulk material properties are considered to vary in the length direction according to the power law distribution. Hamilton's principle is implemented to derive the governing equation of motion and boundary conditions. Considering the surface stress causes that the derived governing equation of motion becomes non-homogeneous while this was not the case in works that only the surface density and the surface Lamé constants were considered. To extract the frequencies of nanorod, firstly the non-homogeneous governing equation is converted to a homogeneous one using an appropriate change of variable, and then for clamped-clamped and clamped-free boundary conditions the governing equation is solved using the harmonic differential quadrature method. Since the present work considers effects of all the surface energy parameters, it can be claimed that this is a comprehensive work in this regard.

Keywords: functionally graded materials; free axial vibration; cracked nanorod; surface energy; harmonic differential quadrature method

1. Introduction

Structures made of functionally graded materials (FGM) are a kind of composite structures in which their mechanical properties gradually vary from a surface to another one. Due to exclusive properties of FGM structures in comparison with homogeneous ones, they are widely used in various fields of technology. Progression of technology in the FGM field makes it possible to fabricate FGM structures in micro/nano-scale. Chemical vapor deposition (Zhang *et al.* 2009), spark plasma sintering (Zheng *et al.* 2005), centrifugal mixed-powder (Watanabe *et al.* 2009), and microwave-assisted (Ashok and Rao 2014) are most common methods of fabrication of homogeneous and non-homogeneous nano-scale structures. Therefore, analysis of this kind of structures due to their highly sensitivity to external stimulations is crucial for accurate design and manufacturing of micro/nano-electro-mechanical systems (MEMS/NEMS).

One of the most useful structures used in MEMS/NEMS is the one-dimensional structures like carbon nanotubes (CNTs). The CNTs can be modelled as nano-beams (Jandaghian and Rahmani 2017, Mirjavadi *et al.* 2017, Rahmani *et al.* 2018, Tagrara *et al.* 2015), nano-bars (Li *et al.* 2017), and nano-rods (Gul *et al.* 2017, Hosseini-Hashemi *et al.* 2017, Nazemnezhad and Kamali 2018b, Oveissi *et al.* 2016). The CNTs are usually modelled as nano-rods when their axial or longitudinal behavior is desired. Literature survey shows that various works have been studied in this regard using different size-dependent theories.

Using the nonlocal elasticity theory, Aydogdu (2012) studied free vibration of thin nanorods embedded in elastic medium and showed the importance of considering the size effect on free axial vibration of nanorods. Nazemnezhad and kamali (Nazemnezhad and Kamali 2018a) analytically investigated inertia of lateral motions and shear stiffness effects on free longitudinal vibration of thick nanorods. Free vibration and wave propagation of nanorods with various geometries and materials, non-uniform and non-homogeneous (Chang 2013), tapered (Danesh *et al.* 2012, Kiani 2010, Şimşek 2012), nanocones (Guo and Yang 2012), axially functionally graded (Nazemnezhad and Kamali 2018b), multiwalled carbon nanotubes (Aydogdu 2014, 2015), viscoelastic (Karličić *et al.* 2015), double-nanorod (Karličić *et al.* 2015, Murmu and Adhikari 2010), are also investigated.

Another size-dependent theory used for analyses of nanostructure behaviors is strain gradient theory. Using this theory, the longitudinal free vibration problem of a micro-scaled bar is formulated (Akgöz and Civalek 2014). Li *et al.* (2016) considered the longitudinal vibration analysis of small-scaled rods in the framework of the nonlocal strain gradient theory. They showed that the nonlocal strain gradient rod model exerts a stiffness-softening effect when

*Corresponding author, Ph.D.
E-mail: rnazemnezhad@du.ac.ir
[a] Ph.D.
E-mail: hshokrollahi@khu.ac.ir

ISSN: 1229-9367 (Print), 1598-6233 (Online)

the nonlocal parameter is larger than the material length scale parameter, and exerts a stiffness-hardening effect when the nonlocal parameter is smaller than the material length scale parameter. In another study, longitudinal free vibration analysis of axially functionally graded microbars is investigated (Akgöz and Civalek 2013). To solve the problem, Rayleigh–Ritz solution technique is utilized and natural frequencies are reported for various cases.

The surface elasticity theory, another well-known size-dependent theory, is also implemented to model axial behavior of nanorods. Nazemnezhad and Shokrollahi (Nazemnezhad and Shokrollahi 2019) investigated free axial vibration of functionally graded materials nanorods with variable cross-section in the framework of this theory. Arefi and Zenkour (2017) focused on analyses of longitudinal wave propagation of FG piezoelectric nanorods. The nanorods were modelled based on Love theory of rods. They reported the effect of different distributions of electric potential on the phase velocity of the nanorod. In a different work, free axial vibration of nanobeams made of aluminum was studied using the surface elasticity theory and the molecular dynamics (MD) simulations (Hosseini-Hashemi *et al.* 2017). In the work, the classic equation of nanobeam in axial vibration was modified by considering the surface elastic moduli and density. This modification caused that the theoretical results agreed very well with those of MD simulations.

It is worth to mention here to some applications of nano-composite structures or nano-scale rod-shaped structures made of functionally graded materials. As the first application it can be mentioned to the application of nano-composite rods in sensors. For example, the ZnO/TiO2 nano-composite rods are synthesized for humidity sensors (Ashok and Rao 2014). The AFG nanobeams are also utilized in atomic force microscopes (Patil *et al.* 2010, Shahba and Rajasekaran 2012). Using the nano-sized spherical- and rod-shaped SiC particles in the nano-composite coatings is the other application of nano-composite rod-shape structures in nanotechnology field (Aal *et al*. 2009).

The above literature survey exhibits that the surface elasticity and strain gradient theories are less utilized in comparison with the nonlocal elasticity theory for axial analyses of nanostructures. In addition, the effect of crack, a common defect in structures, is not comprehensively investigated on axial behavior of nanorods. For these reasons, it is motivated that the free axial vibration of functionally graded materials nanorods in presence of the crack is studied based on the surface elasticity theory. To this end, governing equation of motion and corresponding boundary conditions of cracked FGM (CFGM) nanorods incorporating the surface energy effects are obtained using the Hamilton's principle. Due to considering the surface energy effect the obtained governing equation of motion becomes non-homogeneous. To extract the natural frequencies of the CFGM nanorod, firstly the non-homogeneous governing equation is converted to a homogeneous one using an appropriate change of variable, and then for clamped-clamped and clamped-free boundary conditions the governing equation is solved using an analytical method. In order to have a comprehensive research, effects of various parameters like the variation of material properties, the length and radius of nanorod, the crack severity and position, the type of boundary condition, the values of surface and bulk material properties on axial frequencies of CFGM nanorod are investigated.

2. Problem formulation

Consider a cracked FG nanorod having length L ($0 \le x \le L$) and variable cross section of $S(x)$, in a Cartesian coordinate system xyz, as shown in Fig. 1. As indicated in Fig. 1, a crack is assumed to be located at $x = L_C$.

According to the rod theory, the components of displacement (u, v and w) are as follows (Rao 2007)

$$u(x,y,z,t) = u(x,t) \tag{1}$$

$$v(x,y,z,t) = 0 \tag{2}$$

$$w(x,y,z,t) = 0 \tag{3}$$

in which t is the time in sec. Having these displacements, the strains and stresses can be defined as

$$\varepsilon_{xx} = \frac{\partial u(x,t)}{\partial x} \tag{4}$$

$$\varepsilon_{xy} = \varepsilon_{yy} = \varepsilon_{xz} = \varepsilon_{zz} = \varepsilon_{yz} = 0 \tag{5}$$

$$\sigma_{xx} = E(x)\frac{\partial u(x,t)}{\partial x} \tag{6}$$

$$\sigma_{xy} = \sigma_{yy} = \sigma_{xz} = \sigma_{zz} = \sigma_{yz} = 0 \tag{7}$$

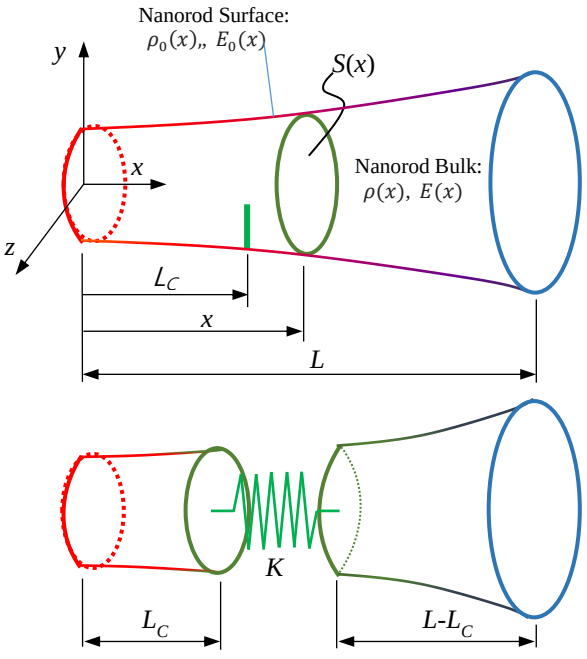

Fig. 1 Schematic of a cracked nanorod and modeled configuration

Eqs. (4)-(7) represent the strains and stresses related to the bulk material of the nanorod. If the surface energy effect is included in the analysis, the surface stress and strain components must be obtained. To this aim, the surface elasticity theory is proposed. In surface elasticity theory proposed by Gurtin and Murdoch (Gurtin and Murdoch 1975), the relation between surface stress and strain can be expressed as

$$\tau_{\alpha\beta}{}^{\pm} = \tau_0{}^{\pm}\delta_{\alpha\beta} + (\mu_0{}^{\pm} - \tau_0{}^{\pm})\left(u_{\alpha,\beta}^{\pm} + u_{\beta,\alpha}^{\pm}\right) + \left(\lambda_0{}^{\pm} + \tau_0{}^{\pm}\right)u_{m,m}\delta_{\alpha\beta} + \tau_0{}^{\pm}u_{\alpha,\beta} \tag{8}$$

$$\tau_{\alpha z}{}^{\pm} = \tau_0{}^{\pm}u_{z,\alpha} \tag{9}$$

in which $\tau_0{}^{\pm}$ is residual surface stress related to no strain condition, $\delta_{\alpha\beta}$ is Kronecker delta, $\lambda_0{}^{\pm}$ and $\mu_0{}^{\pm}$ are Lame constants, $u_{\alpha,\beta}$ are surface displacement components, and $\alpha, \beta = x, y$. Note that the positive and the negative signs are represented for upper and lower surfaces of the nanorod (for rectangular or quadrangular cross sections). Since the nanorod in this study has circular cross section, the positive and negative signs are disregarded.

Using Eqs. (1)-(3), surface stresses effective to longitudinal vibration of nanorod are obtained as

$$\tau_{xx} = \tau_0(x) + \left(\lambda_0(x) + 2\mu_0(x)\right)\frac{\partial u(x,t)}{\partial x} \tag{10}$$

$$\tau_{xy} = \tau_{yy} = \tau_{xz} = \tau_{zz} = \tau_{yz} = 0 \tag{11}$$

The FG nanorod properties, $\mu_0(x)$, $\lambda_0(x)$, $\tau_0(x)$, $\rho_0(x)$, $E(x)$ and $\rho(x)$, as well as its cross section radius $r(x)$, are assumed to change by power law as follows

$$f(x) = f_L + (f_R - f_L)\left(\frac{x}{L}\right)^p;$$
$$f(x) = \lambda_0(x) \text{ or } \mu_0(x) \text{ or } \tau_0(x) \text{ or } \rho_0(x) \text{ or } E(x) \text{ or } \rho(x) \tag{12}$$
$$r(x) = r_L + (r_R - r_L)\left(\frac{x}{L}\right)^q$$

where p is the FG power for the mechanical properties and q is the FG power for the cross-section radius.

In order to arrive to the governing equation and the boundary conditions, the bulk and surface stresses and strains must be used in the Hamilton's principle defined by Eq. (13)

$$\int_{t_1}^{t_2}(\delta KE - \delta PE)dt = 0 \tag{13}$$

The variation of kinetic energy of nanorod takes into account the effect of kinetic energy of surface density, can be written a

$$\begin{aligned}\delta KE &= \delta KE + \delta KE_0 \\ &= \int_0^L \rho(x)\left(\frac{\partial u(x,t)}{\partial t}\right)\delta\left(\frac{\partial u(x,t)}{\partial t}\right)S(x)dx \\ &+ \int_0^L \rho_0(x)\left(\frac{\partial u(x,t)}{\partial t}\right)\delta\left(\frac{\partial u(x,t)}{\partial t}\right)P(x)dx\end{aligned} \tag{14}$$

in which ρ and ρ_0 are bulk and surface density, respectively, and S and P are surface and periphery of nanorod, respectively. Substituting Eqs. (4) and (6) in forming the potential energy relation, the variation of potential energy can be expressed as

$$\begin{aligned}\delta PE = \delta PE + \delta PE_0 &= \int_V \sigma_{xx}\delta\varepsilon_{xx}dV + \int_S \tau_{xx}\delta\varepsilon_{xx}dS \\ &= \int_0^L E(x)\frac{\partial u}{\partial x}\delta\left(\frac{\partial u}{\partial x}\right)S(x)dx \\ &+ \int_0^L \Big(\tau_0(x) \\ &+ \left(\lambda_0(x) + 2\mu_0(x)\right)\frac{\partial u}{\partial x}\Big)\delta\left(\frac{\partial u}{\partial x}\right)P(x)dx\end{aligned} \tag{15}$$

Substituting Eqs. (14) and (15) into Eq. (13), and integrating the resulted equation by part, the governing equation and the corresponding boundary conditions of cracked nanorods incorporating the surface energy effects are obtained as follows

$$\begin{aligned}&-(\rho(x)S(x) + \rho_0(x)P(x))\frac{\partial^2 u(x,t)}{\partial t^2} \\ &+ \frac{\partial}{\partial x}\Big(\tau_0(x)P(x) \\ &+ \Big(E(x)S(x) \\ &+ \left(\lambda_0(x) + 2\mu_0(x)\right)P(x)\Big)\frac{\partial u(x,t)}{\partial x}\Big) = 0\end{aligned} \tag{16}$$

$$\begin{aligned}\tau_{\alpha z}{}^{\pm} = \tau_0{}^{\pm}u_{z,\alpha}\Big(&P(x)\tau_0(x) \\ &+ \Big(E(x)S(x) \\ &+ \left(\lambda_0(x) + 2\mu_0(x)\right)P(x)\Big)\frac{\partial u}{\partial x}\Big)\delta u\Big|_0^L = 0\end{aligned} \tag{17}$$

Assume that in the crack location ($x = L_C$) an equivalent linear spring K connecting the two segments of the nanorod, then for each segment of the nanorod, i.e. $0 \leq x < L_C$ and $L_C < x \leq L$, the Eqs. (16) and (17) must be applied. Implementing Eq. (16) leads to following equations

$$\begin{aligned}&-\left(\rho(x)S(x) + \rho_0(x)P(x)\right)\frac{\partial^2 u_1(x,t)}{\partial t^2} \\ &+ \frac{\partial}{\partial x}\Big(\tau_0(x)P(x) \\ &+ \Big(E(x)S(x) \\ &+ \left(\lambda_0(x) + 2\mu_0(x)\right)P(x)\Big)\frac{\partial u_1(x,t)}{\partial x}\Big) \\ &= 0; \qquad 0 \leq x < L_C\end{aligned} \tag{18}$$

$$\begin{aligned}&-\left(\rho(x)S(x) + \rho_0(x)P(x)\right)\frac{\partial^2 u_2(x,t)}{\partial t^2} \\ &+ \frac{\partial}{\partial x}\Big(\tau_0(x)P(x) \\ &+ \Big(E(x)S(x) \\ &+ \left(\lambda_0(x) + 2\mu_0(x)\right)P(x)\Big)\frac{\partial u_2(x,t)}{\partial x}\Big) \\ &= 0; \qquad L_C < x \leq L\end{aligned} \tag{19}$$

in which, u_1 and u_2 are the axial displacement of the segment located before and after the crack location, respectively.

In crack location, $x = L_C$, following continuity conditions must be satisfied

$$\begin{aligned} K\big(u_1(L_C,t) - u_2(L_C,t)\big) &= -\Big(\tau_0(L_C)P(L_C) \\ &+ \big(E(L_C)S(L_C) \\ &+ \big(\lambda_0(L_C) \\ &+ 2\mu_0(L_C)\big)P(L_C)\big)\frac{\partial u_1(L_C,t)}{\partial x}\Big) \end{aligned} \tag{20}$$

$$\frac{\partial u_1(L_C,t)}{\partial x} = \frac{\partial u_2(L_C,t)}{\partial x} \tag{21}$$

Moreover, end conditions of nanorod for clamped-clamped and clamped-free nanorods are as Eq. (22) and (23) respectively

$$\begin{aligned} u_1(0,t) &= 0 \\ u_2(L,t) &= 0 \\ u_1(0,t) &= 0 \end{aligned} \tag{22}$$

$$\frac{\partial u_2(L,t)}{\partial x} = -\frac{\tau_s(L)S(L)}{E(L)A(L) + \big(\lambda_s(L) + 2\mu_s(L)\big)S(L)} \tag{23}$$

Eqs. (20) and (23) imply that the relation of boundary condition at the free end of the nanorod as well as one of the relations of the continuity conditions are inhomogeneous. Therefore, in order to solve the governing equations of motion, these relations must be homogenized at first.

It is worth mentioning here that it has not been reported in literature that homogeneous relations of boundary conditions and/or equations of motion are changed to inhomogeneous ones by considering the surface energy effects on various mechanical behaviors of nanosized structures. Therefore, the present study reports this issue for the first time.

In order to study the vibration characteristics of the cracked nanorod, Eqs. (18)-(21) along with Eq. (22) and (23) must be solved for the clamped-clamped and the clamped-free conditions, respectively.

As mentioned before, the first step in solving the governing equations of motion is homogenization of Eqs. (20) and (23). At first, the equations and boundary conditions must be homogenized. To this aim it is supposed that

$$u_1(x,t) = v_1(x,t) + \tilde{u}_1(x) \tag{24}$$

$$u_2(x,t) = v_2(x,t) + \tilde{u}_2(x) \tag{25}$$

Substituting $u_1(x,t)$ and $u_2(x,t)$ into Eqs. (18)-(23), the related equations for $\tilde{u}_1(x)$ and $\tilde{u}_2(x)$ are obtained as follows

$$\begin{aligned} \frac{d}{dx}\Big(\tau_0(x)P(x) + \big(E(x)S(x) \\ + \big(\lambda_0(x) + 2\mu_0(x)\big)P(x)\big)\frac{d\tilde{u}_1(x)}{dx}\Big) \\ = 0; \quad 0 \le x < L_C \end{aligned} \tag{26}$$

$$\begin{aligned} \frac{d}{dx}\Big(\tau_0(x)P(x) + \big(E(x)S(x) \\ + \big(\lambda_0(x) + 2\mu_0(x)\big)P(x)\big)\frac{d\tilde{u}_2(x)}{dx}\Big) \\ = 0; \quad L_C < x \le L \end{aligned} \tag{27}$$

$$\begin{aligned} K\big(\tilde{u}_1(L_C) - u_{2cc}(L_C)\big) &= -\Big(\tau_0(L_C)P(L_C) \\ &+ \big(E(L_C)S(L_C) \\ &+ \big(\lambda_0(L_C) + 2\mu_0(L_C)\big)P(L_C)\big)\frac{d\tilde{u}_1(L_C,t)}{dx}\Big) \end{aligned} \tag{28}$$

$$\frac{d\tilde{u}_1(L_C)}{dx} = \frac{d\tilde{u}_2(L_C)}{dx} \tag{29}$$

$$\begin{aligned} &\tilde{u}_2(L) = 0; \text{ for clamped} - \text{clamped nanorod} \\ &\frac{d\tilde{u}_2(L,t)}{dx} \\ &= -\frac{\tau_0(L)P(L)}{E(L)S(L) + \big(\lambda_0(L) + 2\mu_0(L)\big)P(L)}; \text{ for clamped} \\ &- \text{free nanorod} \end{aligned} \tag{30}$$

Solving Eqs. (26)-(30), leads to

$$\begin{aligned} \tilde{u}_1(x) &= \int_0^x \frac{C1 - \tau_0(x)P(x)}{E(x)S(x) + \big(\lambda_0(x) + 2\mu_0(x)\big)P(x)}dx; \\ &for \;\; 0 \le x < L_C \\ C1 &= \frac{K\int_0^L \frac{\tau_0(x)P(x)}{E(x)S(x) + \big(\lambda_0(x) + 2\mu_0(x)\big)P(x)}dx}{1 + K\int_0^L \frac{1}{E(x)S(x) + \big(\lambda_0(x) + 2\mu_0(x)\big)P(x)}dx}; \\ &\text{for clamped} - \text{clamped nanorod} \\ &C1 = 0; \text{ for clamped} - \text{free nanorod} \\ \tilde{u}_2(x) &= \int_{L_C}^x \frac{C1 - \tau_0(x)P(x)}{E(x)S(x) + \big(\lambda_0(x) + 2\mu_0(x)\big)P(x)}dx \\ &+ C2; \quad L_C < x \le L \\ C2 &= -\int_{L_C}^L \frac{C1 - \tau_0(x)P(x)}{E(x)S(x) + \big(\lambda_0(x) + 2\mu_0(x)\big)P(x)}dx; \\ &\text{for clamped} - \text{clamped nanorod} \\ C2 &= -\int_0^{L_C} \frac{\tau_0(x)P(x)}{E(x)S(x) + \big(\lambda_0(x) + 2\mu_0(x)\big)P(x)}dx; \\ &\text{for clamped} - \text{free nanorod} \end{aligned} \tag{31}$$

Now, substituting Eqs. (31) and (32) into Eqs. (24) and (25) and using $u_1(x,t)$ and $u_2(x,t)$ in Eqs. (18)-(23) leads to following equations

$$\begin{aligned} -\big(\rho(x)S(x) + \rho_0(x)P(x)\big)\frac{\partial^2 v_1(x,t)}{\partial t^2} \\ + \frac{\partial}{\partial x}\Big(\big(E(x)S(x) \\ + \big(\lambda_0(x) + 2\mu_0(x)\big)P(x)\big)\frac{\partial v_1(x,t)}{\partial x}\Big) = 0; \quad 0 \\ \le x < L_C \end{aligned} \tag{33}$$

$$-\big(\rho(x)S(x)+\rho_0(x)P(x)\big)\frac{\partial^2 v_2(x,t)}{\partial t^2} + \frac{\partial}{\partial x}\Bigg(\Big(E(x)S(x) + \big(\lambda_0(x)+2\mu_0(x)\big)P(x)\Big)\frac{\partial v_2(x,t)}{\partial x}\Bigg) = 0;\quad L_C < x \le L \tag{34}$$

$$K\big(v_1(L_C,t)-v_2(L_C,t)\big) = -\Big(E(L_C)S(L_C) + \big(\lambda_0(L_C)+2\mu_0(L_C)\big)P(L_C)\Big)\frac{\partial v_1(L_C,t)}{\partial x} \tag{35}$$

$$\frac{\partial v_1(L_C,t)}{\partial x} = \frac{\partial v_2(L_C,t)}{\partial x} \tag{36}$$

$$v_1(0,t)=0$$
$$v_2(L,t)=0;\ \text{for clamped}-\text{clamped nanorod}$$
$$\frac{\partial v_2(L,t)}{\partial x}=0;\ \text{for clamped}-\text{free nanorod} \tag{37}$$

Assuming harmonic displacements as

$$v_1(x,t)=V_1(x)T(t)=V_1(x)e^{i\omega t} \tag{38}$$

$$v_2(x,t)=V_2(x)T(t)=V_2(x)e^{i\omega t} \tag{39}$$

Eqs. (33)-(37) can be rewritten as

$$\omega^2\big(\rho(x)A(x)+\rho_0(x)S(x)\big)V_1(x) + \frac{d}{dx}\Bigg(\Big(E(x)A(x) + \big(\lambda_0(x)+2\mu_0(x)\big)S(x)\Big)\frac{dV_1(x)}{dx}\Bigg) = 0;\quad 0 \le x < L_C \tag{40}$$

$$\omega^2\big(\rho(x)A(x)+\rho_0(x)S(x)\big)V_2(x) + \frac{d}{dx}\Bigg(\Big(E(x)A(x) + \big(\lambda_0(x)+2\mu_0(x)\big)S(x)\Big)\frac{dV_2(x)}{dx}\Bigg) = 0;\quad L_C < x \le L \tag{41}$$

$$K\big(V_1(L_C)-V_2(L_C)\big) = -\Big(E(L_C)A(L_C) + \big(\lambda_0(L_C)+2\mu_0(L_C)\big)S(L_C)\Big)\frac{dV_1(L_C)}{dx} \tag{42}$$

$$\frac{dV_1(L_C)}{dx} = \frac{dV_2(L_C)}{dx} \tag{43}$$

$$V_1(0)=0$$
$$V_2(L)=0;\ \text{for clamped}-\text{clamped nanorod}$$
$$\frac{dV_2(L)}{dx}=0;\ \text{for clamped}-\text{free nanorod} \tag{44}$$

As can be seen from Eqs. (40)-(44), the surface energy parameters appear in the governing equations of motion, Eqs. (40) and (41), as well as in the continuity condition, Eq. (42). However, the boundary conditions, Eqs. (43) and (44), are the same for both the surface elasticity and classical theory. Furthermore, the equation of motion of the conventional rod can be obtained from Eqs. (40) and (41) by setting $\rho_0 = \lambda_0 = \mu_0 = 0$. It should be noted that the obtained governing equations, Eqs. (40) and (41), clearly show that including surface effect in formulations leads to an increase in the stiffness of the nanorod, for positive values of $\lambda_0 + 2\mu_0$. Moreover, according to Eqs. (31) and (32) the residual surface stress, τ_0, is the cause of the time-independent components for displacements, i.e., $\tilde{u}_1(x)$ and $\tilde{u}_2(x)$. A precise looking at these components suggests that $\tilde{u}_1(x)$ and $\tilde{u}_2(x)$ are non-positive values indicating the residual surface stress is a cause of stiffer behavior of the nanorod.

Solving Eqs. (40)-(44) numerically, using differential quadrature method (DQM), the natural frequencies of the clamped-clamped cracked nanorod are obtained. The application of DQ method was well presented in Refs. (Nazemnezhad and Hosseini-Hashemi 2014, Nazemnezhad *et al.* 2014); it is presented briefly here.

For solving the obtained equations, the HDQM is used. In this method, the derivative of a function, with respect to a spatial variable at a given discrete point, approximated by a linear summation of weighted function values at all discrete points chosen in the solution domain of the spatial variable. Suppose the domain of considered nanorod are represented by ($0<x< L$) and being discretized by N_x grid points along x coordinate. Then the derivatives of $F(x)$ with respect to x at the point (x_i) can be expressed discretely as

$$\frac{d^n F(x_i)}{dx^n} = \sum_{k=1}^{N_x} A_{ik}^{(n)} F(x_k);\ n = 1,2,\dots,N_x-1; \tag{45}$$

where $A_{ik}^{(n)}$ are the weighting coefficients in conjunction to the order of derivative of F(x) with respect to x, i.e. n at the discrete points x_i. The description of HDQ method and how to choose the positions of the grid points using Chebyshev polynomials can be found in detail in Ref. (Civalek 2004). Now, the HDQM can be used to discretize the coupled Eqs. (40)-(44). After separating domain and boundary degrees of freedom (DOF), the following assembled matrix equations are obtained

$$\begin{bmatrix}[K_{bb}] & [K_{bd}]\\ [K_{db}] & [K_{dd}]\end{bmatrix}\begin{Bmatrix}\{d^b\}\\ \{d^d\}\end{Bmatrix} = \omega^2\begin{Bmatrix}0\\ \{d^d\}\end{Bmatrix} \tag{46}$$

where $\{d^b\}$ and $\{d^d\}$ represent the boundary and domain DOF, respectively. After doing some mathematical simplifications on Eq. (46), the frequencies of the CFGM nanorod can be calculated by solving the following relation

$$\big[[K_{dd}]-[K_{db}][K_{bb}]^{-1}[K_{bd}]\big]\{d^d\} = \omega^2\{d^d\} \tag{47}$$

Based on the above outlined formulations, and by aids of the MATLAB program solver a self-developed computer program is written by which the natural frequencies of the CFGM nanorod can be obtained.

Table 1 Non-dimensional fundamental frequencies of intact axially FGM nanorod.

Boundary condition	Fixed-Fixed		Fixed-Free	
E_{ratio}	Şimşek (2012)	Present study	Şimşek (2012)	Present study
0.25	2.3424	2.34227	1.3455	1.34551
0.50	2.6774	2.67747	1.4359	1.43600
1.00	3.1416	3.14159	1.5708	1.57080
2.00	3.7865	3.78651	1.7657	1.76570
4.00	4.6848	4.68455	2.0413	2.04117

Table 2 Natural frequencies of intact axially FGM nanorod with surface effects (GHz)

L (nm)	Mode	Fixed-Fixed		Fixed-Free	
		Present study	Nazemnezhad and Shokrollahi (2019)	Present study	Nazemnezhad and Shokrollahi (2019)
10	1	310.836	310.944	214.072	214.072
	2	640.145	640.422	505.595	505.614
	3	964.420	965.026	819.570	819.681
15	1	207.224	207.296	142.714	142.715
	2	426.764	426.948	337.064	337.076
	3	642.947	643.351	546.380	546.454
20	1	155.418	155.472	107.036	107.036
	2	320.073	320.211	252.798	252.807
	3	482.210	482.513	409.785	409.840

Table 3 The surface and bulk mechanical properties of functionally graded cracked nanorod

E_L (GPa)	E_R (GPa)	ρ_L (kg/m^3)	ρ_R (kg/m^3)	ρ_{0_L} $(\mu kg/m^2)$	ρ_{0_R} $(\mu kg/m^2)$	λ_{0_L} (N/m)	λ_{0_R} (N/m)	μ_{0_L} (N/m)	μ_{0_R} (N/m)
210	70	2370	2700	0.317	0.546	-5.0985	6.8420	-2.7779	-0.8269

3. Results and discussion

3.1 Comparison study

Before presentation of numerical and graphical results, a comparison study is conducted to verify the applicability and accuracy of the present formulation. Due to the lack of the similar problem and solution concerning the crack effect on the axial vibration of axially FGM nanorods, the accuracy of the present solution is verified by comparing the results with those of Şimşek (2012) for an intact axially FGM tapered nanorod incorporating nonlocal effect (see Table 1) and Nazemnezhad and Shokrollahi (Nazemnezhad and Shokrollahi 2019) for an intact axially FGM nanorod incorporating surface effect (see Table 2). In Table 1 the non-dimensional fundamental frequency ($\lambda = \omega L\sqrt{(A_L\rho_L)/(A_L E_L)}$) of fixed-fixed and fixed-free intact axially FGM nanorod are compared. The values of some parameters are $\mu(nonlocal\ parameter) = 0;\quad p = 1;$ $\rho_{ratio} = \rho_R/\rho_L = 1;\quad q = 0$. And in Table 2 natural frequencies of FGM nanorod with fixed-fixed and fixed-free boundary conditions are listed for various mode numbers and nanorod lengths. The mechanical properties are considered to be identical to the values reported in Ref. (Nazemnezhad and Shokrollahi 2019), for an intact axially FGM nanorod with R = 1.5 nm and p = 2. As shown in

Tables 1 and 2, the reliability of the present formulation and results is confirmed. It is worth to note that the small difference between the results of the present formulation and those of Refs. (Şimşek 2012) and (Nazemnezhad and Shokrollahi 2019) is due to the solution method used. The present work is used the numerical method, HDQ method, while Refs. (Şimşek 2012) and (Nazemnezhad and Shokrollahi 2019) are used the analytical method, Galerkin's method.

3.2 Benchmark results

After verifying the applicability and accuracy of the present formulation, the effects of some parameters on natural frequency of CFGM nanorod are investigated. In all following case studies, the mechanical surface and bulk properties are considered as presented in Table 3. It is worth to note that the following abbreviations are used in the figures and tables

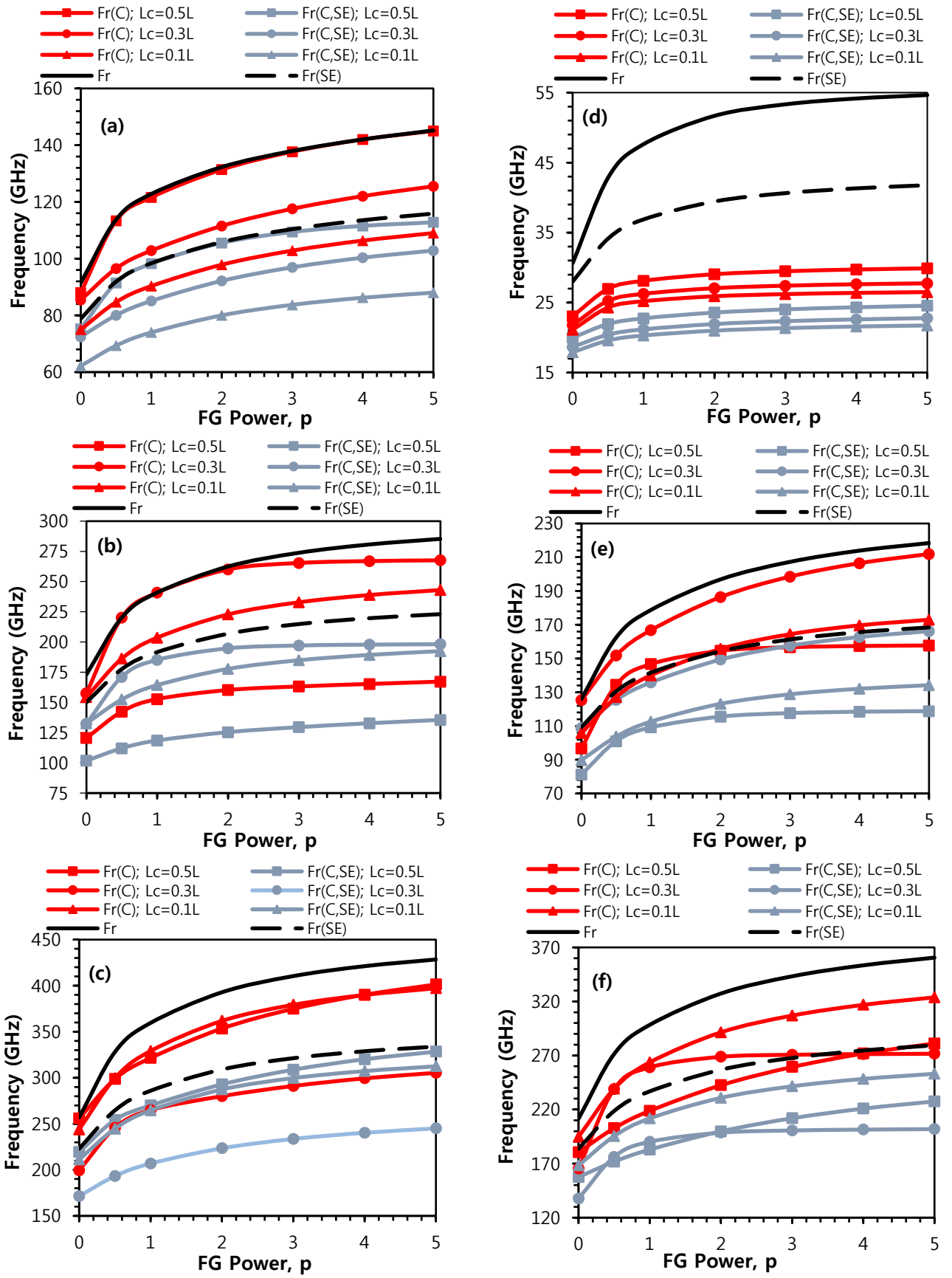

Fig. 2 Variations of frequency versus the FG power for various crack locations; (a) 1st mode, fixed-fixed, (b) 2nd mode, fixed-fixed, (c) 3rd mode, fixed-fixed, (d) 1st mode, fixed-free, (e) 2nd mode, fixed-free and (f) 3rd mode, fixed-free (C = 2; q = 2; R_L = 0.5 nm; R_R = 1 nm; L = 30 nm)

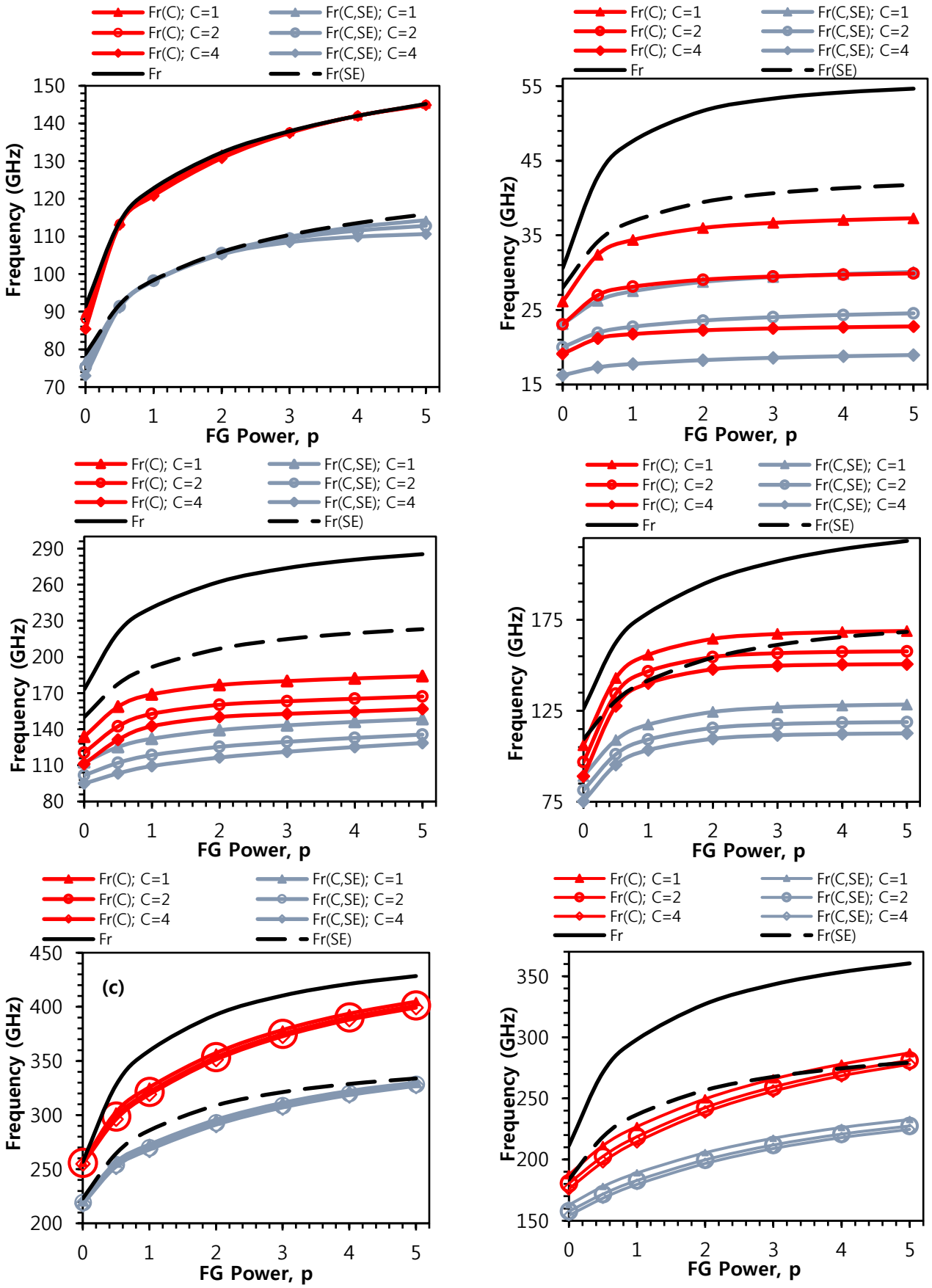

Fig. 3 Variations of frequency versus the FG power for various values of crack severity parameter, (a) 1st mode, fixed-fixed, (b) 2nd mode, fixed-fixed, (c) 3rd mode, fixed-fixed, (d) 1st mode, fixed-free, (e) 2nd mode, fixed-free and (f) 3rd mode, fixed-free (Lc =L/2; q = 2; R_L = 0.5 nm; R_R = 1 nm; L = 30 nm)

Fr = Classical frequency

Fr (SE) = Frequency with surface effects, no crack

Fr (C) = Frequency without surface effect, with crack (48)

Fr (C,SE) = Frequency with surface and crack effects

Firstly, variations of the first three natural frequencies versus the FG power are demonstrated in Figs. 2(a)-2(f) for various crack locations (L_c) and two types of boundary conditions, fixed-fixed and fixed-free. Figs. 2(a)-2(f) show that since Fr(C) and Fr(SE) curves are located below the Fr curve for all values of the FG power, it can be concluded that both the crack and the surface energy have decreasing effects on axial frequencies of CFGM nanorods. This is due to this fact that both of them decrease the stiffness of the CFGM nanorod. It is also seen from Figs. 2(a)-2(f) that the axial frequencies increase by increasing the FG power. This is because of increasing the values of the mechanical properties of the CFGM nanorod by increasing the FG power. Comparison of Figs. 2(a)-2(f) shows that the crack effect is strongly dependent on the frequency number (since the mode shape of a given frequency number is different from the others), crack location and boundary condition. Another point of Figs. 2(a)-2(f) is that the distance between Fr and Fr(SE) curves increases by increasing the FG power. This implies that the decreasing effect of the surface energy increases by increasing the FG power.

Secondly, variations of axial frequencies versus the FG power are plotted in Figs. 3(a)-3(f) for various crack severities and fixed-fixed and fixed-free boundary conditions. Since some conclusions of Figs. 3(a)-3(f) are similar to those observed from Figs. 2(a)-2(f), new observations are only explained here. Figs. 3(a)-3(f) show that if the crack does not have any decreasing effect on the axial frequencies, a change in the value of the crack severity cannot alters this situation. On the other hand, the decreasing effect of crack increases by increasing the crack severity. The other result of Figs. 3(a)-3(f) is that the Fr(C) or Fr(C,SE) curves have a constant distance for various values of the FG power. This means that the decreasing effect of crack with a given crack severity is independent from the FG power. The last point of Figs. 3(a)-3(f) is that the decreasing effect of crack due to a change in its severity is not the same for CFGM nanorods with different boundary conditions.

Next, we turn our attention to considering the effects of crack and surface energy on the axial frequencies for various radii of CFGM nanorod. To this end, Figs. 4(a)-4(f) are provided. It is worth to mention that the FG power for the cross-section radius is q=2. It can be seen from Figs. 4(a)-4(f) that axial frequencies of CFGM nanorods are dependent on the radius while this is not the case for homogeneous nanorods (Rao 2007). This conclusion is also true for CFGM nanorods with crack and surface energy. Another point of Figs. 4a-4f is that the axial frequencies are more for thicker CFGM nanorods with and without crack and surface energy effects. This difference becomes more at higher values of FG power p. Figs. 4(a)-4(f) also display that the dependency of the axial frequencies of the CFGM nanorods on the radius is different for various mode numbers. Therefore, it is difficult to express a distinct trend. The results presented are valid for both types of boundary conditions, fixed-fixed and fixed-free.

In this section, we consider variations of axial frequencies versus the FG power for various values of the CFGM nanorod length (see Figs. 5(a)-5(f)). The first point of Figs. 5(a)-5(f) is that the axial frequencies of CFGM nanorods are dependent on the length as it is observed for homogeneous nanorods (Rao 2007). Figs. 5a-5f show that the axial frequencies of CFGM nanorod decrease by increasing its length. This is due to this fact that as the CFGM nanorod increases, its stiffness decreases and its mass increases. In addition, it can be observed from Figs. 5(a)-5(f) that the reduction of axial frequencies of longer CFGM nanorods is more at higher values of FG power p. Comparison of the difference between Fr and Fr(SE) curves implies that the surface energy has more decreasing effect on the axial frequencies of CFGM nanorods with shorter lengths. This is also true for the decreasing effect of the crack. Another comparison can be made between Fr(SE) and Fr(C) curves. Figs. 5(a)-5(f) exhibit that in some cases Fr(SE) curves are located below the Fr(C) curves while in some others it is vice versa. This implies that it cannot be definitely stated that which factor, the crack or the surface energy, has a dominant effect on the axial frequencies of the CFGM nanorods. The results presented are valid for both types of boundary conditions, fixed-fixed and fixed-free.

At the final part of this section, we introduce new parameters to investigate effects of the crack and the surface energy parameters on the axial frequencies of CFGM nanorods in another way. The new parameters are

- The ratio of frequency with only crack to the classical frequency $FR(C) = Fr(C)/Fr$
- The ratio of frequency with crack and surface density (ρ_0) to the classical frequency $FR(C,\rho_0) = Fr(C,\rho_0)/Fr$
- The ratio of frequency with crack and surface Lame constant (λ_0) to the classical frequency $FR(C,\lambda_0) = Fr(C,\lambda_0)/Fr$ (49)
- The ratio of frequency with crack and surface energy parameters (ρ_0 and λ_0) to the classical frequency $FR(C,SE) = Fr(C,SE)/Fr$

Based on the parameters defined in Eq. (49) Figs. 6a and 6b and Table 4 are provided. It is observed from Figs. 6a and 6b that all FR curves are located below the line FR=1. This reconfirms that the surface energy and the crack have decreasing effects on the axial frequencies of the CFGM nanorods. Figs. 6(a) and 6(b) also give some new interesting points. The first interesting point is that the FR(C,ρ_0) curve is located below the FR(C,λ_0) one. This means that however value of the surface density is much less than the value of the surface Lame constant (λ_0), its decreasing effect on the axial frequencies of the CFGM nanorods is more. This is valid for both boundary conditions considered here and for all mode numbers. Another interesting point from Figs. 6a and 6b is that if we assume that the crack is located where it has its maximum decreasing effect, then we can conclude that at low values of the crack severity, the surface energy has dominant decreasing effects on the axial frequencies of the CFGM

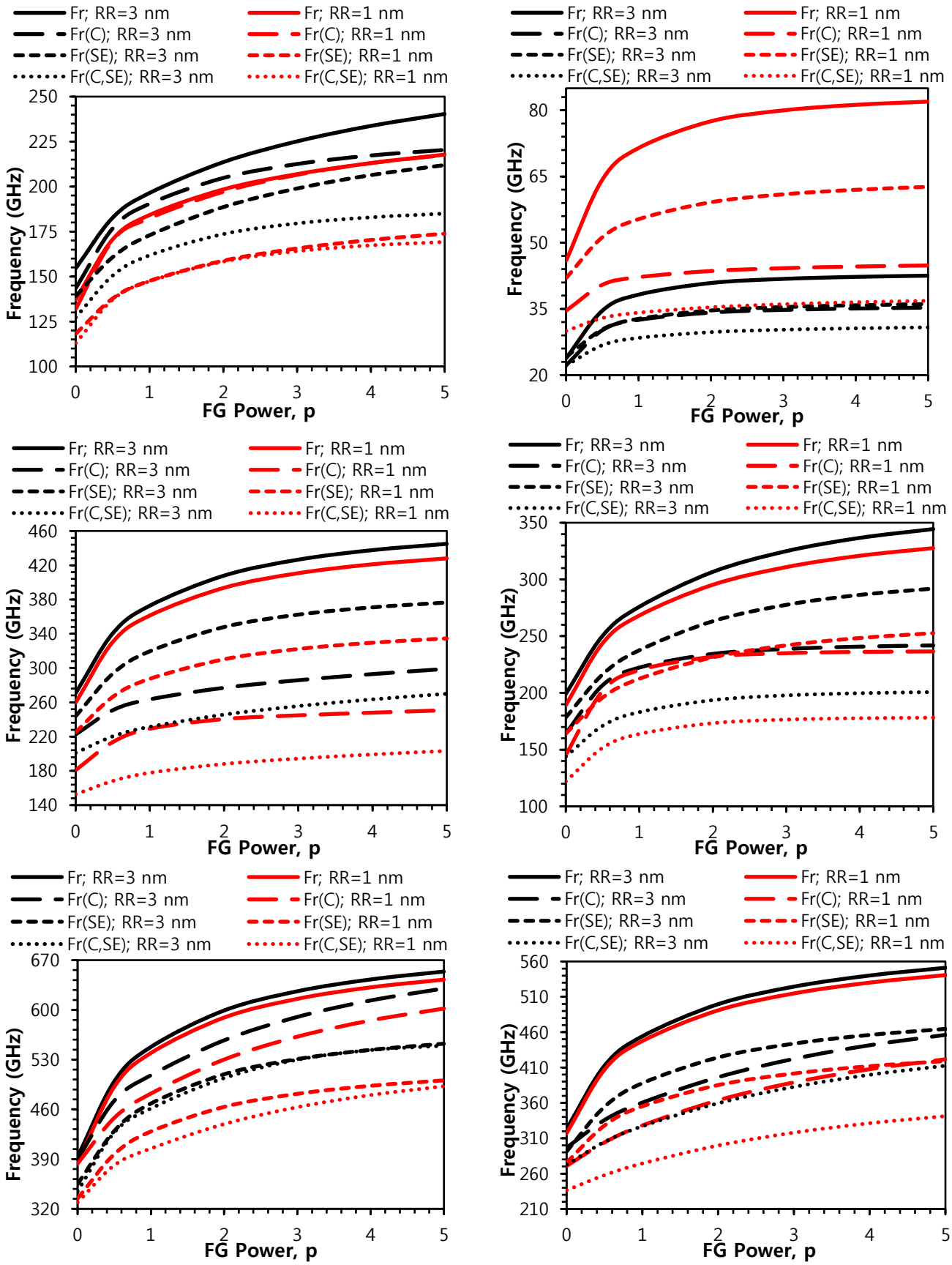

Fig. 4 Variations of frequency versus the FG power for various values of nanorod radius (R_R); (a) 1st mode, fixed-fixed, (b) 2nd mode, fixed-fixed, (c) 3rd mode, fixed-fixed, (d) 1st mode, fixed-free, (e) 2nd mode, fixed-free and (f) 3rd mode, fixed-free (C=2; Lc =L/2; q = 2; R_L = 0.5 nm; L = 20 nm).

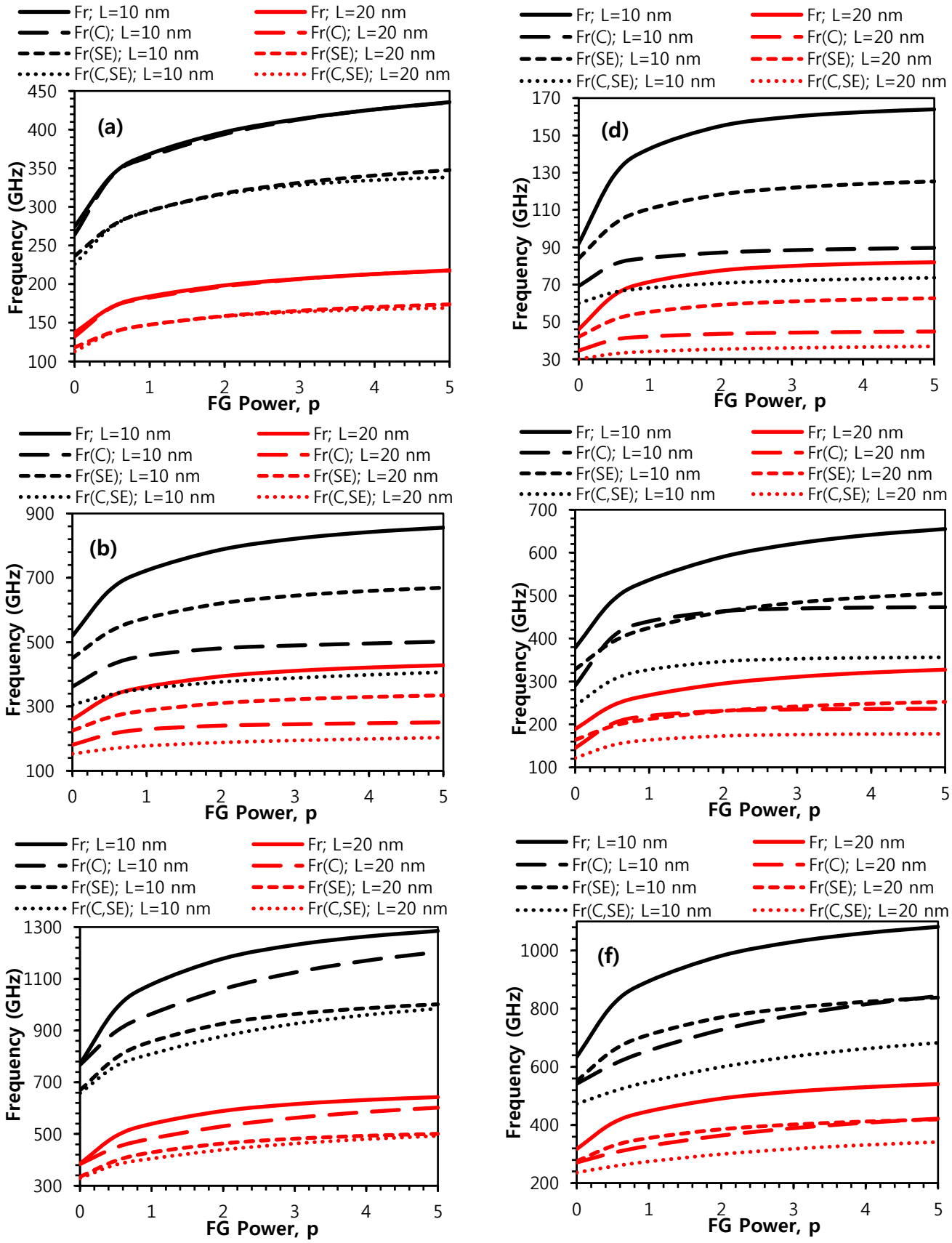

Fig. 5 Variations of frequency versus the FG power for various values of nanorod length (L); (a) 1st mode, fixed-fixed, (b) 2nd mode, fixed-fixed, (c) 3rd mode, fixed-fixed, (d) 1st mode, fixed-free, (e) 2nd mode, fixed-free and (f) 3rd mode, fixed-free (C=2; Lc =L/2; q = 2; R_L = 0.5 nm; R_R = 1 nm)

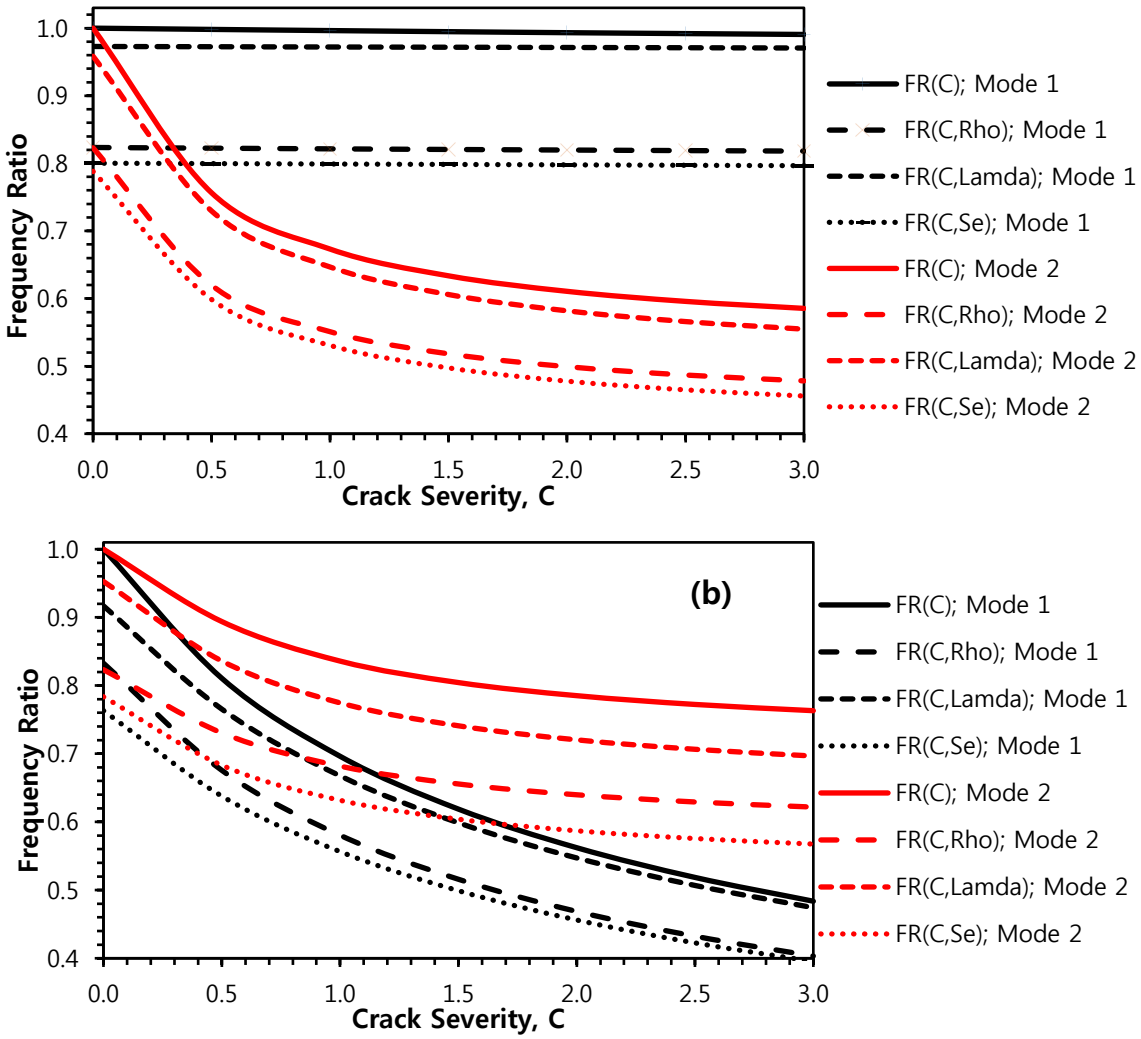

Fig. 6 Variations of frequency ratios versus the crack severity for various cases; (a) fixed-fixed and (b) fixed-free (Lc =L/2; q = 2; R_L = 0.5 nm; R_R = 1 nm; L = 30 nm; p=2).

Table 4 Values of frequency ratios for various cases

BC	n	C	P=0			P=1			P=10		
			FR(C,ρ_0)	FR(C,λ_0)	FR(C,SE)	FR(C,ρ_0)	FR(C,λ_0)	FR(C,SE)	FR(C,ρ_0)	FR(C,λ_0)	FR(C,SE)
Fixed-Fixed	1	0.0	0.78003	1.10323	0.86155	0.81106	0.98919	0.80114	0.83999	0.94292	0.79074
		0.5	0.76974	1.09395	0.85118	0.80957	0.98912	0.80087	0.83277	0.93111	0.77736
		1.0	0.75981	1.08467	0.84114	0.80817	0.98905	0.80060	0.82554	0.91942	0.76469
		1.5	0.75054	1.07570	0.83178	0.80685	0.98898	0.80033	0.81880	0.90878	0.75376
		2.0	0.74209	1.06725	0.82331	0.80562	0.98890	0.80005	0.81281	0.89960	0.74478
	2	0.0	0.78181	1.10810	0.86700	0.81247	0.98009	0.79558	0.83703	0.93295	0.78056
		0.5	0.67074	0.91783	0.72087	0.63380	0.76492	0.61817	0.60528	0.69480	0.58411
		1.0	0.60959	0.82477	0.64991	0.56452	0.67913	0.54847	0.54258	0.62279	0.52564
		1.5	0.57407	0.77377	0.61144	0.53005	0.63544	0.51315	0.51573	0.59127	0.50044
		2.0	0.55163	0.74252	0.58811	0.50964	0.60908	0.49191	0.50146	0.57443	0.48709
Fixed-Free	1	0.0	0.81136	1.12601	0.91394	0.82556	0.93862	0.77440	0.85145	0.90367	0.76930
		0.5	0.74725	1.01321	0.82440	0.68590	0.79485	0.65656	0.68144	0.74779	0.63797
		1.0	0.69456	0.92603	0.75446	0.59669	0.69893	0.57755	0.58077	0.64857	0.55374
		1.5	0.65073	0.85683	0.69860	0.53437	0.63010	0.52074	0.51371	0.57961	0.49503
		2.0	0.61376	0.80052	0.65297	0.48792	0.57790	0.47762	0.46524	0.52844	0.45140
	2	0.0	0.78084	1.11002	0.86763	0.81242	0.97625	0.79220	0.83272	0.91984	0.76538
		0.5	0.70030	0.99333	0.76732	0.74238	0.87735	0.70581	0.67176	0.75427	0.62311
		1.0	0.64755	0.91949	0.70687	0.69888	0.81862	0.65656	0.61469	0.68748	0.56720
		1.5	0.61283	0.87289	0.66956	0.67332	0.78449	0.62844	0.58782	0.65435	0.53965
		2.0	0.58881	0.84163	0.64481	0.65707	0.76284	0.61076	0.57239	0.63484	0.52346

nanorods while it is the other way round at high values of the crack severity for the decreasing effect of the crack. There is also an interesting point from Table 4. This table shows that for p=0 and C=0, the value of FR(C,λ_0) is more than one. This exhibits that the surface Lame constant (λ_0) can increase the axial frequencies of CFGM nanorods if p=0. This is due to this fact that for p=0, the nanorod is only made of the material considered for the right end of the nanorod. Table 4 shows that the value of the surface lame constant (λ_0) for the right end of the nanorod is positive while it is the other way round for the value of the surface lame constant (λ_0) at the left end of the nanorod. In general, since the decreasing or increasing effect of the surface Lame constant (λ_0) is much less than the decreasing effect of the surface density, we can conclude that the surface energy has always a decreasing effect on the axial frequencies of homogeneous and CFGM nanorods.

5. Conclusions

Effects of the crack and the surface energy on the free longitudinal vibration of functionally graded nanorods are investigated. The surface and bulk material properties are considered to vary in the length direction according to the power law distribution. Considering the surface stress causes that the derived governing equation of motion becomes non-homogeneous while this was not the case in works that only the surface density and the surface Lamé constants were considered. After converting the non-homogeneous governing equation to the homogeneous one, natural frequencies are obtained using the numerical method, the harmonic differential quadrature method. The results reveal that both the crack and the surface energy decrease the axial frequencies of the CFGM nanorods. The decreasing effect of the crack with a given crack severity is independent from the FG power while the decreasing effect of the surface energy increases by increasing the FG power. In addition, it is concluded that at low values of the crack severity, the surface energy has dominant decreasing effects on the axial frequencies of the CFGM nanorods while it is the other way around at high values of the crack severity for the decreasing effect of the crack. It is also observed that however value of the surface density is much less than the value of the surface Lamé constant (λ_0), its decreasing effect on the axial frequencies of the CFGM nanorods is more for both boundary conditions and for all mode numbers. The surface Lamé constant (λ_0) may decrease or increase the axial frequencies of CFGM nanorods which it is dependent on the sign of λ_0. The results also show that the axial frequencies of CFGM nanorods are dependent on the length as it is observed for homogeneous nanorods. Furthermore, the axial frequencies of CFGM nanorods are dependent on the radius while this is not the case for homogeneous nanorods. The dependency of the axial frequencies of the CFGM nanorods on the radius is different for various mode numbers. Therefore, it is difficult to express a distinct trend. Finally, it cannot be definitely stated that which factor, the crack or the surface energy, has a dominant effect on the axial frequencies of the CFGM nanorods.

References

Aal, A.A., El-Sheikh, S. and Ahmed, Y. (2009), "Electrodeposited composite coating of Ni–W–P with nano-sized rod-and spherical-shaped SiC particles", *Mater. Res. Bull.*, **44**(1), 151-159. https://doi.org/10.1016/j.materresbull.2008.03.008.

Akgöz, B. and Civalek, Ö. (2013), "Longitudinal vibration analysis of strain gradient bars made of functionally graded materials (FGM)", *Compos. Part B: Eng.*, **55**, 263-268. https://doi.org/10.1016/j.compositesb.2013.06.035.

Akgöz, B. and Civalek, Ö. (2014), "Longitudinal vibration analysis for microbars based on strain gradient elasticity theory", *J. Vib. Control*, **20**(4), 606-616. https://doi.org/10.1177/1077546312463752.

Arefi, M. and Zenkour, A.M. (2017), "Employing the coupled stress components and surface elasticity for nonlocal solution of wave propagation of a functionally graded piezoelectric Love nanorod model", *J. Intel. Mat. Syst. Str.*, **28**(17), 2403-2413. https://doi.org/10.1177/1045389X17689930.

Ashok, C. and Rao, K.V. (2014), "ZnO/TiO2 nanocomposite rods synthesized by microwave-assisted method for humidity sensor application", *Superlattices and Microstruct.*, **76**, 46-54. https://doi.org/10.1016/j.spmi.2014.09.029.

Aydogdu, M. (2012), "Axial vibration analysis of nanorods (carbon nanotubes) embedded in an elastic medium using nonlocal elasticity", *Mech. Res. Commun.*, **43**, 34-40. https://doi.org/10.1016/j.mechrescom.2012.02.001.

Aydogdu, M. (2014), "Longitudinal wave propagation in multiwalled carbon nanotubes", *Compos. Struct.*, **107**, 578-584. https://doi.org/10.1016/j.compstruct.2013.08.031.

Aydogdu, M. (2015), "A nonlocal rod model for axial vibration of double-walled carbon nanotubes including axial van der Waals force effects", *J. Vib. Control*, **21**(16), 3132-3154. https://doi.org/10.1177/1077546313518954.

Chang, T.P. (2013), "Axial vibration of non-uniform and non-homogeneous nanorods based on nonlocal elasticity theory", *Appl. Math. Comput.*, **219**(10), 4933-4941. https://doi.org/10.1016/j.amc.2012.11.059.

Civalek, Ö. (2004), "Application of differential quadrature (DQ) and harmonic differential quadrature (HDQ) for buckling analysis of thin isotropic plates and elastic columns", *Eng. Struct.*, **26**(2), 171-186. https://doi.org/10.1016/j.engstruct.2003.09.005.

Danesh, M., Farajpour, A. and Mohammadi, M. (2012), "Axial vibration analysis of a tapered nanorod based on nonlocal elasticity theory and differential quadrature method", *Mech. Res.*, **39**(1), 23-27. *https://doi.org/10.1016/j.mechrescom.2011.09.004.*

Gul, U., Aydogdu, M. and Gaygusuzoglu, G. (2017), "Axial dynamics of a nanorod embedded in an elastic medium using doublet mechanics", *Compos. Struct.*, **160**, 1268-1278. https://doi.org/10.1016/j.compstruct.2016.11.023.

Guo, SQ. and Yang, S.P. (2012), "Axial vibration analysis of nanocones based on nonlocal elasticity theory", *Acta Mechanica Sinica*, **28**(3), 801-807. https://doi.org/10.1007/s10409-012-0109-4.

Gurtin, M.E. and Murdoch, A.I. (1975), "A continuum theory of elastic material surfaces", *Archive for Rational Mechanics and Analysis*, **57**(4), 291-323. https://doi.org/10.1007/BF00261375.

Hosseini-Hashemi, S., Fakher, M. and Nazemnezhad, R. (2017), "Longitudinal vibrations of aluminum nanobeams by applying elastic moduli of bulk and surface: molecular dynamics simulation and continuum model", *Mater. Res. Express*, **4**(8), 085036.

Jandaghian, A.A. and Rahmani, O. (2017), "Vibration analysis of FG nanobeams based on third-order shear deformation theory under various boundary conditions", *Steel Compos. Struct.*, **25**(1), 67-78. https://doi.org/10.12989/scs.2017.25.1.067.

Karličić, D., Cajić, M., Murmu, T. and Adhikari, S. (2015), "Nonlocal longitudinal vibration of viscoelastic coupled double-nanorod systems", *Eur. J. Mech.-A/Solids*, **49**, 183-196. https://doi.org/10.1016/j.euromechsol.2014.07.005.

Kiani, K. (2010), "Free longitudinal vibration of tapered nanowires in the context of nonlocal continuum theory via a perturbation technique", *Physica E: Low-Dimensional Syst. Nanostruct.*, **43**(1), 387-397. https://doi.org/10.1016/j.physe.2010.08.022.

Li, L., Hu, Y. and Li, X. (2016), "Longitudinal vibration of size-dependent rods via nonlocal strain gradient theory", *Int. J. Mech. Sci.*, **115-116**, 135-144. https://doi.org/10.1016/j.ijmecsci.2016.06.011.

Li, X.F., Tang, G.J., Shen, Z.B. and Lee, K.Y. (2017), "Size-dependent resonance frequencies of longitudinal vibration of a nonlocal Love nanobar with a tip nanoparticle", *Math. Mech. Solids*, **22**(6), 1529-1542. https://doi.org/10.1177/1081286516640597.

Mirjavadi, S.S., Afshari, B.M., Shafiei, N., Hamouda, A. and Kazemi, M. (2017), "Thermal vibration of two-dimensional functionally graded (2D-FG) porous Timoshenko nanobeams", *Steel Compos. Struct.*, **25**(4), 415-426. https://doi.org/10.12989/scs.2017.25.4.415.

Murmu, T. and Adhikari, S. (2010), "Nonlocal effects in the longitudinal vibration of double-nanorod systems", *Physica E: Low-Dimensional Syst. Nanostruct.*, **43**(1), 415-422. https://doi.org/10.1016/j.physe.2010.08.023.

Nazemnezhad, R. and Hosseini-Hashemi, S. (2014), "Free vibration analysis of multi-layer graphene nanoribbons incorporating interlayer shear effect via molecular dynamics simulations and nonlocal elasticity", *Physics Lett. A*, **378**(44), 3225-3232. https://doi.org/10.1016/j.physleta.2014.09.037.

Nazemnezhad, R. and Kamali, K. (2018a), "An analytical study on the size dependent longitudinal vibration analysis of thick nanorods", *Mater. Res. Express*, **5**(7), 075016.

Nazemnezhad, R. and Kamali, K. (2018b), "Free axial vibration analysis of axially functionally graded thick nanorods using nonlocal Bishop's theory", *Steel Compos. Struct.*, **28**(6), 749-758. https://doi.org/10.12989/scs.2018.28.6.749.

Nazemnezhad, R. and Shokrollahi, H. (2019), "Free axial vibration analysis of functionally graded nanorods using surface elasticity theory", *Modares Mech. Eng.*, **18**(9), 131-141.

Nazemnezhad, R., Shokrollahi, H. and Hosseini-Hashemi, S. (2014), "Sandwich beam model for free vibration analysis of bilayer graphene nanoribbons with interlayer shear effect", *J. Appl. Phys.*, **115**(17), 174303. ttps://doi.org/10.1063/1.4874221.

Oveissi, S., Eftekhari, S.A. and Toghraie, D. (2016), "Longitudinal vibration and instabilities of carbon nanotubes conveying fluid considering size effects of nanoflow and nanostructure", *Physica E: Low-Dimensional Syst. Nanostruct.*, **83**, 164-173. https://doi.org/10.1016/j.physe.2016.05.010.

Patil, A.V., Beker, A.F., Wiertz, F.G., Heering, H.A., Coslovich, G., Vlijm, R. and Oosterkamp, T.H. (2010), "Fabrication and characterization of polymer insulated carbon nanotube modified electrochemical nanoprobes", *Nanoscale*, *2*(5), 734-738.

Rahmani, O., Hosseini, S., Ghoytasi, I. and Golmohammadi, H. (2018), "Free vibration of deep curved FG nano-beam based on modified couple stress theory", *Steel Compos. Struct.*, **26**(5), 607-620. https://doi.org/10.12989/scs.2018.26.5.607.

Rao, S.S. (2007). *Vibration of Continuous Systems*: John Wiley & Sons.

Shahba, A. and Rajasekaran, S. (2012), "Free vibration and stability of tapered Euler–Bernoulli beams made of axially functionally graded materials", *Appl. Math. Model.*, **36**(7), 3094-3111. https://doi.org/10.1016/j.apm.2011.09.073.

Şimşek, M. (2012), "Nonlocal effects in the free longitudinal vibration of axially functionally graded tapered nanorods", *Comput. Mater. Sci.*, **61**, 257-265. https://doi.org/10.1016/j.commatsci.2012.04.001.

Tagrara, S., Benachour, A., Bouiadjra, M.B. and Tounsi, A. (2015), "On bending, buckling and vibration responses of functionally graded carbon nanotube-reinforced composite beams", *Steel Compos. Struct.*, **19**(5), 1259-1277. https://doi.org/10.12989/scs.2015.19.5.1259.

Watanabe, Y., Inaguma, Y., Sato, H. and Miura-Fujiwara, E. (2009), "A novel fabrication method for functionally graded materials under centrifugal force: The centrifugal mixed-powder method", *Materials*, **2**(4), 2510-2525. https://doi.org/10.3390/ma2042510.

Zhang, T., Kumari, L., Du, G., Li, W., Wang, Q., Balani, K. and Agarwal, A. (2009), "Mechanical properties of carbon nanotube–alumina nanocomposites synthesized by chemical vapor deposition and spark plasma sintering", *Compos. Part A: Appl. Sci. Manufact.*, **40**(1), 86-93. https://doi.org/10.1016/j.compositesa.2008.10.003.

Zheng, Y., Wang, S., You, M., Tan, H. and Xiong, W. (2005), "Fabrication of nanocomposite Ti (C, N)-based cermet by spark plasma sintering", *Mater. Chem. Phys.*, **92**(1), 64-70. https://doi.org/10.1016/j.matchemphys.2004.12.031.

CC